

# The Second Level Topological Trigger of the H1 Experiment at HERA I

D. Hoffmann<sup>a</sup>, E. Banaś<sup>b</sup>, C. Beigbeder<sup>c</sup>, R. Bernier<sup>c</sup>,  
D. Breton<sup>c</sup>, J. C. Bizot<sup>c</sup>, A. Ducorps<sup>c</sup>, L. Goerlich<sup>b</sup>,  
M. Jacquet<sup>c</sup>, J. Martyniak<sup>b</sup>, S. Mikocki<sup>b</sup>, G. Nowak<sup>b</sup>,  
J. Turnau<sup>b</sup>

<sup>a</sup> *Centre de Physique des Particules, IN2P3/CNRS, Université de la  
Méditerranée, Marseille, France*

<sup>b</sup> *Institute for Nuclear Physics, Cracow, Poland*

<sup>c</sup> *Laboratoire de l'Accélérateur Linéaire, IN2P3/CNRS, Université de Paris-Sud,  
Orsay, France*

---

## Abstract

Since the end of the 1995 HERA running period the second level topological trigger (L2TT) of the H1 experiment is in operation. The L2TT trigger decision is based on the topological event signatures derived from subdetector signals, which are projected onto a  $16 \times 16$  Boolean matrix representing the geometry of the detector in the  $(\theta, \phi)$  space. A special ASIC has been developed for performing this analysis. The decision of the L2TT is delivered within  $20 \mu s$  allowing the computation of correlations of trigger data in high granularity. Calorimeter information is compared to a set of consecutive thresholds and combined in a flexible manner with track and muon data. 16 L2TT signals are sent to the central trigger logic in order to validate first level (L1) trigger information. This allows optimization of the signal to noise ratio for various physics processes.

---

## 1 Introduction

Since May 1992 the first ever constructed electron-proton storage ring HERA has been in operation. Electrons<sup>1</sup> of 27.5 GeV energy collide in this accelerator with 820 GeV protons<sup>2</sup> allowing studies of a wide area of physics processes to be extended into a previously unexplored kinematic region of lepton-nucleon

---

<sup>1</sup> In this paper, the generic term "electron" is used for electrons and positrons.

<sup>2</sup> The proton beam energy has been increased to 920 GeV as of August 1998.

and photon-nucleon scattering. H1 [1] is one of the two colliding beam experiments at HERA designed to exploit this unique opportunity.

In order to achieve the high luminosity required for precision measurements and the investigation of rare processes in electron-proton interactions, the two colliding beams consist of bunch trains of protons and electrons crossing each other at a rate of 10.4 MHz. The short time distance of 96 ns between collisions and requirements of minimizing dead time forced a pipelining of all data in the front-end readout systems of the experiment.

The variety of physics processes under study in  $ep$  collisions at HERA covers a broad range of cross sections and consequently of rates, extending from a few events per week to thousands of events per second. The induced background, mainly originating from the interaction of the proton beam with the construction part of the machine (beam wall collisions) and with the residual gas in the beam pipe (beam gas collisions), can produce event rates of the order of 100 kHz, by far exceeding the rate of interesting physics events. The asymmetric beam energies of HERA frequently leads to strongly forward<sup>3</sup> boosted events that are hard to distinguish from the proton beam induced background.

In order to enhance the physics-to-background ratio and to separate with high efficiency the specific physics channels from background, two independent second level (L2) trigger systems [2], operating in parallel, were incorporated into the existing trigger scheme at the end of the 1995 running period: a neural network trigger [3] and a topological trigger [4]. The chosen implementation and flexible logic of the L2 trigger have enabled fast and easy response to changing demands on the trigger system imposed by varying beam conditions and physics requirements. Thus it became possible to trigger rare physics channels even in the presence of large competing background processes.

We are describing the concept, realization and performance of the L2 topological trigger (L2TT) until the upgrade [5] shutdown of the HERA accelerator in the year 2001. Since then, several subdetectors and the trigger, data acquisition and logging system have undergone various changes, which cannot be considered here. This article is organized as follows. The H1 detector and its trigger system are introduced in Sec. 2. Information available at the L2 trigger is described in Sec. 3. In Sec. 4 the general principles of the trigger algorithm are presented. The L2TT hardware is described in Sec. 5. The structure and loading of the steering file is presented in Sec. 6 together with tools for monitoring and testing of the L2TT behaviour and for the development of new selection criteria. In Sec. 7 some examples of the trigger applications for different physics channels are shown. We conclude with a short summary.

---

<sup>3</sup> The forward region is defined with respect to the proton beam direction.

## 2 The H1 detector and its trigger system

### 2.1 The H1 detector

The H1 detector [1] is a general purpose system composed of a number of complex subdetectors. Starting the description from the interaction vertex, the detector consists of a silicon tracker for precision measurements of charged particles and vertices. It is surrounded by a tracking system of interleaved multiwire proportional chambers (MWPCs) and drift chambers (CJCs), providing the primary track measurement of charged particles. A big liquid argon cryostat surrounds the trackers. It houses a highly segmented liquid argon (LAr) calorimeter with an electromagnetic and a hadronic section containing a total of about 45,000 channels. A superconducting cylindrical coil with a diameter of 6 m provides the magnetic field for transverse momentum measurement. The iron return yoke of the magnet is instrumented with limited streamer tube chambers for muon identification. Muon tracks in the forward direction are measured in drift chambers surrounding a toroidal magnet. A lead scintillating-fibre (called “spaghetti”) calorimeter (SpaCal) [6] enables precise measurement of the scattered electron in the backward direction. Additional small calorimeters and taggers, situated along the beam line at certain distances from the detector in both directions, provide measurements of particles at very low angle and of the luminosity delivered to the experiment.

### 2.2 The H1 trigger and DAQ system

The H1 trigger and acquisition system consists of four different levels of decision of which two, the first level (L1) trigger and the asynchronous online filtering (L4), have been in operation since the start of data taking. The pipelined L1 trigger [7] runs deadtime free and is phase-locked to the HERA clock signal (HClk) of 10.4 MHz. It provides a delayed decision after  $2.3 \mu\text{s}$  for each bunch crossing. The subdetector systems feed data into front-end pipelines. A subset of these data is used by most systems to generate fast information about general properties of the event. This is encoded in Boolean decisions known as *trigger elements*. Up to 256 trigger elements can be sent to the L1 logic of the central trigger (CTL1). The central trigger system then provides the decision on acceptance of each possible event. It is made on the basis of 128 different logical combinations of the trigger elements, known as *subtriggers*. They are formed using RAM look-up tables, thus giving a maximum of flexibility. Because of the reduced bandwidth, subtriggers with too high rate need to be restricted. This is achieved by prescaling, i.e. only every  $n$ th positive subtrigger decision is accepted. The logical OR of all 128 prescaled subtrig-

gers constitutes the final L1 trigger decision. A number of sets of subtriggers and prescale factors are defined and adjusted semiautomatically ensuring low deadtime and allowing the acceptance for both low and high rate processes to be optimized simultaneously for evolving beam conditions that occur during one accelerator fill [8].

An L1 'accept' decision (L1\_keep signal) stops the front-end pipelines and the primary deadtime starts to accumulate. The L1\_keep decision is then validated by the subsequent trigger levels. The second level trigger is provided with part of the raw trigger data of the different L1 trigger subsystems which form a quick separate data stream independent of the main detector readout. It delivers a result within 20  $\mu$ s. This time limit enables complex correlations of trigger data from different subdetectors, which are carried out with a much higher granularity than in the L1 trigger. The L2 decision is derived from two independent hardware systems [2]. Each of them generates up to 16 L2 trigger elements which are sent to the central trigger level 2 decision logic (CTL2). Logical combinations of the L2 trigger elements form subtriggers which are used to validate specific L1 subtriggers. A positive L2 decision starts the readout of the front-end data, which takes slightly more than 1 ms on average, whereas an L2 reject signal allows the pipelines to be re-enabled. If the L1 and L2 trigger accept rates do not exceed 1 kHz and 50 Hz respectively,<sup>4</sup> then H1 is able to run with an overall deadtime below 10%. The fourth trigger level (L4), a RISC processor farm [9] acts asynchronously as a filter on the full data to reduce their logging rate and volume [10]. It reconstructs most of the event properties and takes decisions on the quality of the events. The output of the L4 selection is written to tape at a typical rate of 5 – 10 events per second.

### 3 Input data to the L2TT

All the information used by the L2TT system is provided at L1\_keep. The following subdetectors (cf. Fig. 1) contribute to the L2TT decision: the LAr and the SpaCal calorimeters, the central drift chambers, the forward (FPC) and central inner (CIP) and outer (COP) proportional chambers, and the forward and central muon detectors. In addition to the subdetector information, all the L1 subtrigger bits are sent to the L2TT. The generation and the meaning of the different subdetector information before transmission to the L2 systems are described in this section.

---

<sup>4</sup> The third level (L3) trigger was not used until 2004 and the required reduction of the input rate to the next level (L4) was achieved by L2 alone.

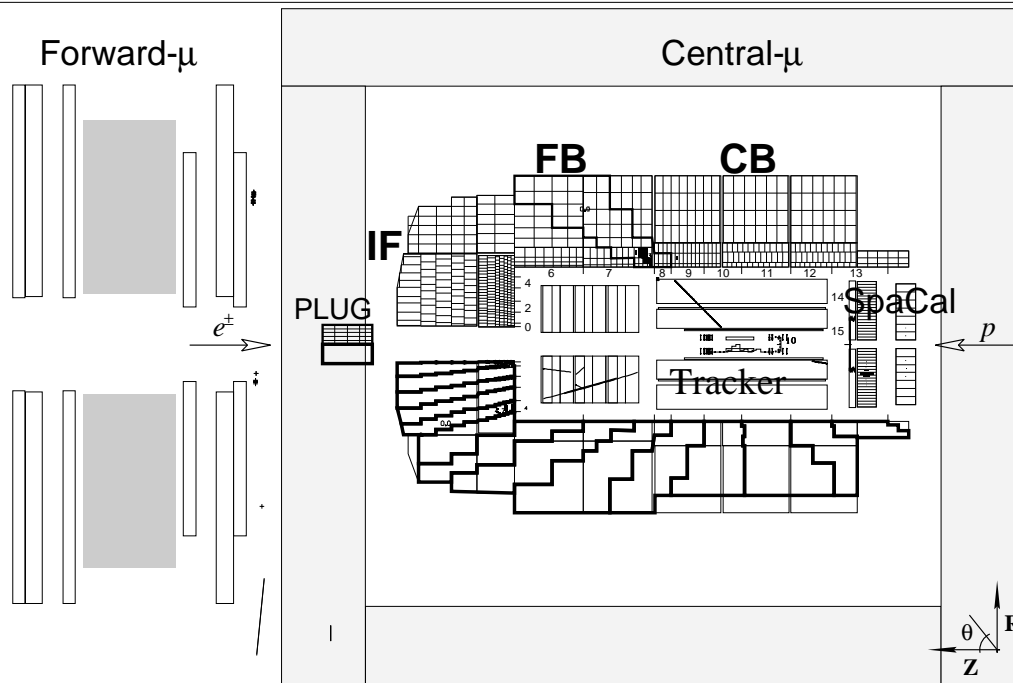


Fig. 1. Cross section through the  $\theta$  plane of the H1 detector, showing the subdetectors which are used by the L2TT system: This figure shows the trackers around interaction point and beam-axis schematically in an  $rz$ -projection. The calorimeters and their segmentation are drawn around the central and forward tracking chambers. We distinguish three calorimeters from the forward ( $+z$ ) to the backward direction: The PLUG calorimeter, the Liquid Argon calorimeter with the IF, FB and CB partitions and the SpaCal. The cell structure is shown in the upper ( $+r$ ) part, the BT segmentation along the polar angle  $\theta$  is shown in the lower part of the calorimeters (thick lines). The BT  $\Theta$ -Indices are numbered  $0 \dots 15$ . All these central subdetectors are surrounded by the central muon chambers (light gray). The forward direction is further instrumented with a big toroid magnet (gray) and associated drift chambers.

### 3.1 Calorimeter data

The *liquid argon calorimeter trigger* [11] is designed to deliver local information about energy deposits in various parts of the calorimeter as well as the total energy and other global energy sums. The calorimeter is coarsely segmented in *big towers* (BTs) along the polar angle  $\theta$  and the azimuthal angle  $\phi$  (cf. Fig. 1 and Table 1). Each BT delivers the summed signal of the calorimeter cells in its  $\theta$ - $\phi$  region to a Flash-ADC (FADC). The 8 bit energy information sent to L2, separately for electromagnetic and hadronic parts, represents energies of 0 to approximately 30 GeV on a linear scale. Particles with higher energies are only seen at the energy saturation level by all triggers. A total of 240 BTs are formed from the LAr cells with the calorimeter divided into 14

intervals in  $\theta$ . Each  $\theta$  interval corresponds a  $\Theta$ -index  $\Theta = 0 \dots 13$  as shown in Fig. 1. Another 8 BTs with  $\Theta$ -indices 14 and 15 are derived in a similar way from the signals of the SpaCal. The  $\phi$ -segmentation varies for different  $\Theta$ -indices as shown in Table 1.

Table 1

Varying  $\phi$ -granularity for LAr Big Towers (BT) as a function of the  $\Theta$ -index number

partition	IF					FB					CB			SpaCal		
$\Theta$ -index	0	1	2	3	4	5	6	7	8	9	10	11	12	13	14	15
$\phi$ -gran.	8	16	16	32	32	16	16	16	16	16	16	16	16	8	4	4

The *inclusive electron trigger* (IET) [6] for the backward direction is provided by the SpaCal. It is built from  $4 \times 4$  energy sums over neighbouring electromagnetic cells, which are read out in the time-of-flight window for  $ep$  interactions. The energy sums are performed in overlapping sliding windows matching in size the Molière radius [12] of the SpaCal to avoid inefficiency at the window boundary. They are compared to three programmable thresholds in a range from 0.5 GeV to 20 GeV and thus deliver three cluster bits per sliding window. A map of cluster bits is sent to the L2 systems. Details on the available thresholds and very good spatial resolution, which is in the best case only four times smaller than that of the full data, are given in Table 2, which summarizes all calorimeter data available for the L2 trigger subsystems.

Table 2

Calorimeter data, which are fed into the L2 trigger subsystems

Detector	Input data ( <b>Calorimeter part</b> )
LAr	<ul style="list-style-type: none"> <li>energies of individual big towers, separately for electromagnetic and hadronic sections (Only 8-bit values above a zero-suppression threshold are transmitted and limited to a total of 210 bytes.)</li> </ul>
SpaCal	<ul style="list-style-type: none"> <li>fine map of cluster bits for the 2<sup>nd</sup> threshold (384 bits),</li> <li>cluster bits of the central part for three thresholds (48 bits),</li> <li>local ORs of 16 cluster bits for three thresholds (72 bits)</li> </ul>

### 3.2 Tracking information

The *central jet chamber trigger* (DCr $\phi$  trigger [13]) uses ten radial layers of the CJC wires to find tracks in the  $r\phi$ -plane which have a distance of closest approach of less than 2 cm to the nominal beam axis. The  $r\phi$ -plane is divided into 45 sectors and the  $\phi$  position of a track (4 bits/sector) is sent to the L2, whereby tracks with transverse momentum  $p_t$  *low* ( $400 \text{ MeV} < p_t < 800 \text{ MeV}$ ) or *high*, ( $p_t > 800 \text{ MeV}$ ) can be distinguished as well as the charge of the tracks.

The *z-vertex trigger* [14] processes the signals from six CIP and COP layers and the first module of the FPC. A *z-vertex* histogram with 16 bins along  $z$  is filled with the  $z$  coordinates at  $r=0$  of *rays*, straight-line coincidences in the  $rz$ -plane of MWPC hits. The histogram bin with the largest number of entries (peak position) above the relatively flat background from random coincidences is associated with the interaction vertex of a possible  $ep$  collision. All entries to the histogram, peak position and its height and two quality numbers are sent to the L2 systems.

The *forward ray trigger* [15] combines the signals of the three FPC modules and the CIP. Unlike in the *z-vertex* trigger, a ray is here defined as a set of impacts on three or four chambers, compatible with a track coming from the interaction region.

These rays, which are found by the forward ray trigger and the *z-vertex* trigger, and are pointing to the peak of the *z-vertex* histogram, are grouped into the coarser granularity of *big rays* (BRs), which is matched to the BT granularity of the liquid argon calorimeter trigger. This allows the correlation of these two detector types. A BR map is sent to the L2 systems.

Table 3  
Track data, which are fed into the L2 trigger subsystems

Detector	Input data ( <b>Tracker part</b> )
CJC	<ul style="list-style-type: none"> <li>• <math>\phi</math> position of tracks with 45fold granularity for negative and positive tracks with low and high <math>p_t</math> (180 bits)</li> </ul>
MWPC	<ul style="list-style-type: none"> <li>• big ray map in 14 <math>\theta</math>-bins <math>\times</math> 16 <math>\phi</math>-bins (224 bits),</li> <li>• all entries in the <i>z-vertex</i> histogram (12 bits),</li> <li>• peak height (8 bits) and position (4 bits),</li> <li>• 2 quality bits</li> </ul>
Central $\mu$	<ul style="list-style-type: none"> <li>• hit map of barrel and endcap modules (64 bits)</li> </ul>
Forward $\mu$	<ul style="list-style-type: none"> <li>• combined track and pre-toroid information for octants (128 bits)</li> </ul>

The *central muon trigger* [16] applies various coincidence conditions on the digitized output of five trigger layers of the instrumented iron for indicating a muon track candidate in a detector module to the L1 trigger. The instrumented iron system is divided into four subdetectors: forward and backward barrels, and forward and backward endcaps. Each of them consists of 16 modules. One bit per module indicates to the L2 systems where a muon hit is detected.

The *forward muon trigger* [17] is based on information from the forward muon spectrometer, consisting of two sets of chambers before the forward iron toroid and two sets after it. The spectrometer is divided into 8 octants subdivided into eight radial regions. The pre- and post-toroid information is combined to

find tracks which have traversed the magnet. This information together with the pre-toroid one is sent to the L2.

A summary of the tracking information sent to the L2 trigger systems is given in Table 3.

### 3.3 L2 trigger data transmission and signal paths

The L2 decision must be delivered within 20  $\mu$ s of the L1\_keep decision. This has motivated the development of two special bus standards for the transmission of the L2 trigger data, which correspond to two different algorithms of data compression: Quickbus and PQZP system. They allow all L2 trigger data to be received within 5  $\mu$ s of L1\_keep.

The Calorimeter BT data are transferred via Quickbus and zero-suppressed before transmission. Values below a partition dependent threshold are not sent. This data reduction is paid with an overhead in volume (for the addresses) and time (3 HClk/word) in the hardware, which was designed in the early nineties [18]. The Quickbus is a 14 bit (6-bit address + 8-bit value) asynchronous handshake protocol bus with RS-242 signals.

All other subdetectors use the PQZP system [19], which allows the choice between an optionally zero-suppressed Quickbus and the PQZPbus, which is not zero-suppressed. The PQZPbus is a 16-bit synchronous bus clocked at the HClk frequency. Its signals are differential ECL, known within H1 as “H1 differential” standard [20].

The complete connection scheme of subdetector triggers and the L2 systems is outlined in Fig. 2: All BT values and partial calorimeter energy sums are transmitted through Quickbusses to a Quickbus Receiver in the L2 systems. All other subsystems deliver their trigger data through PQZP standard busses to a PQZPbus Receiver card [21]. This transmission is triggered by an L1\_keep signal. The average data size of one transmission (one *L2 event*) is less than 400 16-bit-words. The Quickbus Receiver and the PQZPbus Receiver are used to distribute an L2 event over eight parallel synchronous 16-bit busses (L2busses) on the J2 backplane (see Sec. 5.1) at the rate of  $8 \times 16$ -bit words per HClk in a freely programmable way. One or several of these L2busses are connected to the specific acquisition cards (see Sec. 5.3) of the L2TT system, which filter out and translate the relevant information of the L2 data.

In this way it was possible to use the same data transmission and reception hardware for all L2 subsystems, thus granting high reliability and conformity. A Spy card for checking and monitoring the traffic on the L2busses was developed as a standard utility board for the L2 triggers.

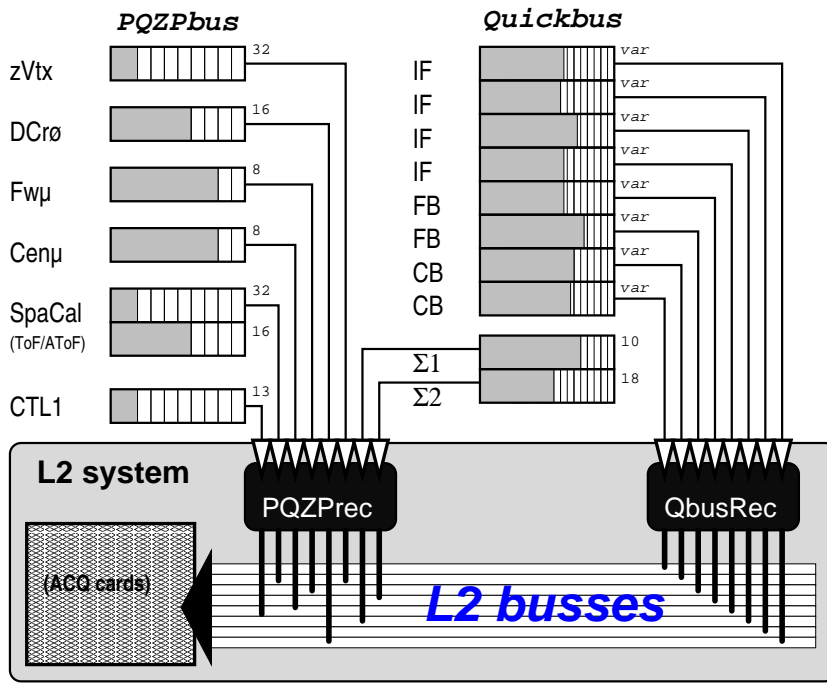


Fig. 2. Data transmission scheme of the L2 trigger data through the PQZPbus (upper left), 7 data channels with a total of 125 16-bit words, and the Quickbus (upper right), 8 busses with variable data length (due to zero-suppression and with a maximum of 16 words) from the calorimeter FADCs and 2 constant length busses for partial calorimeter energy sums

#### 4 General principles of the L2TT

The topological trigger algorithm is based on the determination and the examination of different event signatures derived from the input signals described in Sec. 3. For this the input signals are projected on a  $16 \times 16$  Boolean matrix representing the detector geometry in the  $(\theta, \phi)$  space. The basic principle can be illustrated by the picture of a draughts game (Fig. 3), which represents the L2TT view of the event display in Fig. 1. The drafts represent calorimeter (BT) energies from different partitions, track trigger signals or any logical combination of these. The 16 decisions corresponding to the L2 trigger elements delivered by the L2TT differ by the way to select, weight and combine these ingredients. Assuming that we consider pure BT energy information in a first time, we represent the BT energy in every square by a tower of draughts in the checkerboard field, which has the BT  $\Theta$ - and  $\Phi$ -indices as its coordinates. Our algorithm simplifies the BT energy scale of the 8-bit FADC values by attributing a 3-bit *energy index* (0 to 7) to each value, that is typically a logarithmically rising function of these. Two energy indices will be used to characterize the event in the trigger, which finds:

- the BT(s) with maximal energies (highest stacks(s) of draughts pieces)

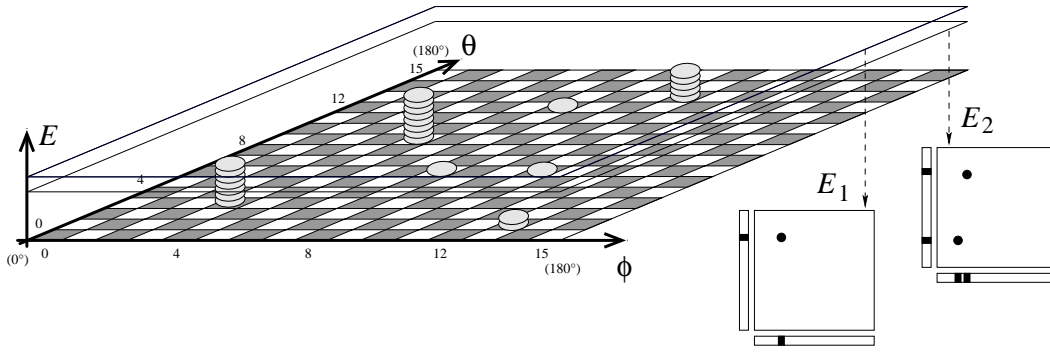


Fig. 3. **Chequerboard illustration of the L2TT algorithm.** Seven deposits of energy are represented on the board by towers of stacked draughts, each of them representing a well defined energy unit, that can vary locally. Only the highest tower exceeds the first energy level  $E_1$ . Its projection on the  $\phi$  and  $\theta$  axes gives one entry in each of the sidebars. When the threshold is lowered to  $E_2$ , the second tower appears with two entries in the  $\phi$  and  $\theta$  projection.

above the threshold selected by the highest energy index  $E_1$ , called *the primary energy index*,

- and in the case of a *trivial topology*, where only one tower reaches the energy level  $E_1$ , an additional *secondary energy index*  $E_2$ , which is the highest index with a different topology.

For our example in Fig. 3 it would work out as follows: Starting from the maximum energy index, only the highest tower exceeds the first energy level where the projections are not empty,  $E_1$ . It has a trivial topology, as its projection on the  $\phi$  and  $\theta$  axes gives a single entry in each of the sidebars. When the threshold is lowered to  $E_2$ , the second tower appears. The L2TT algorithm stops the analysis of this phase then. Hence it doesn't see the third important tower and all other low energy deposits generated for example by detector noise. For each energy index it extracts respectively:

- the projection onto the  $\Phi$  and  $\Theta$  axis of all towers with energies above threshold,
- the number, size and relative positions of clusters and some more variables as explained later (cf. Sec. 5.4).

The towers can be built up from any logical combination of electromagnetic and hadronic BTs and combined with track information projected on a Boolean  $\Theta$ - $\Phi$  matrix with fixed granularity. Due to the time constraints for the execution of the algorithm, only a selection of all possible signal combinations are programmed into the hardware components. We define up to 128 families, which are identified by two numbers: *family*  $F \in \{0, \dots, 15\}$  and *sub-family*  $f \in \{0, \dots, 7\}$ , and the data correlation rules for each family may vary locally (per calorimeter partition). Reduced in this way, the L2 input data of an event are still significant enough to distinguish between physics channels

and background. The family numbers and the energy index  $E$  together form a *mapping condition*, which determines the analysis subspace in which, and the way how, we consider the event in our trigger during a given step of the algorithm. An additional code, the *projection selection*  $P \in \{0, \dots, 3\}$ , defines how the Boolean matrix is projected onto the  $\Theta$  and  $\Phi$  axis in regions without 1:1 correspondence between the Calorimeter BT map and the Boolean  $16 \times 16$  matrix. Hence every family has a primary and secondary energy index with the associated  $\Theta$  and  $\Phi$  projections, which characterize the event signature by their L2 data. Considering that the trigger electronics can extract values for different mapping conditions ( $E; F; P$ ) at a 10 MHz rate, it becomes obvious that not all of them can be computed within the limited L2 decision time. The reduction of the number of possible projections and the choice of the relevant cases is essential for the implementation of the L2TT algorithm.

The mapping conditions are chosen in order to yield a significant discrimination between physics and background. A *distance to background* value is attributed to a given mapping. It is calculated as a linear function of the energy index, by means of a lookup table, where also any other function can be implemented. The parameters of the algorithm must be optimized in order to give larger distance to background values for those topological signatures which are typical for physics events, than for those who represent the background type of events. Several mapping conditions usually enter the calculation of each L2TT element. The sum of all distances corresponding to these mappings is compared to a predetermined threshold depending on the trigger element. If this sum, considered as the *total distance to background* is greater than this threshold, then the corresponding trigger element is set true.

The L2 analysis must be finished within  $20 \mu\text{s}$  i. e. 208 HClk periods including the acquisition of information (cf. Sec. 3.3). The event is examined by the L2TT in four phases:

- phase 0 — reception of data from subdetectors in the acquisition cards
- phase 1 — analysis of calorimeter information in order to determine the energy indices of some key correlations with calorimeter signals only,
- phase 2 — analysis of different mappings, computation of the distance to background values for each mapping and increment of the corresponding distance sum counter,
- phase 3 — comparison of the total distance to background value for each trigger element with its predefined threshold, transmission of the trigger elements to the central trigger and eventually transmission of the history of the analysis to the Monitor card (cf. Sec. 6).

The trigger can examine up to 70 event mappings for each L1\_keep event. The central CPU must request every mapping, wait for the result, interpret it and, depending on this, initiate the analysis of further mappings. The parallelized

algorithm is described in detail in Sec. 5.5.2 and needs in average time of less than 5 CPU cycles, per mapping condition, thus taking  $11.2 \mu\text{s}$  in total for phases 1 and 2. Additional time is devoted to initialization of the machinery (phase 0) and final result computation (phase 3).

## 5 Hardware implementation

### 5.1 Overview

The hardware consists of two VME [22] crates (cf. Fig. 4 and [23]): a 9U crate which contains the main L2TT electronics and a Monitoring crate which is 6U high and completely conforms to the VME32 standard. The 9U Trigger

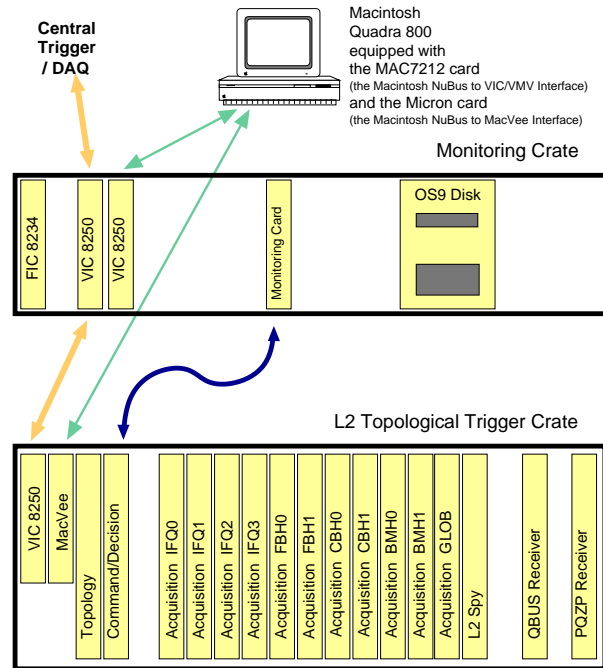


Fig. 4. Crate layout of the L2TT system: The Trigger crate (bottom) contains all electronic modules, which are necessary for the L2TT trigger function. The detailed description of the VME modules is given in Sec. 5. The Monitoring crate (center) is used as an independent, local DAQ system (cf. Sec. 6.2). Both crates are setup by a Macintosh computer (on top of the crates in this figure), to which they are connected by a VICbus and MacVEE connection.

Crate contains a 16 bit VME bus for all slots at the position of J1 and a VME32 bus (J1+J2) only for the first two slots. This frees the J2 backplane for the L2busses (Sec. 3.3), which distribute the subdetector data to the Acquisition (ACQ) cards. J3 is used for an L2TT bus between the ACQ and Topology (TOP) cards. The TOP card and the Command-Decision card are the main

parts of the system. The eleven Acquisition cards are identical except for the programming of some of their ROMs. Up to two PQZPbus Receiver cards and up to two Quickbus Receiver cards receive the data of an L2 event sent by the various subdetectors as described in Sec. 3.3.

Control and loading of the trigger are done from a Macintosh Quadra 800 (*Mac* for short) which is connected to the Trigger Crate via a NuBus/MacVEE connection and to the Monitoring crate with a VICbus [24]. The readout for the H1 Central DAQ during luminosity data taking is performed by the Central Trigger Processor for the L2 and L3 systems CTPL23, which is connected to both crates through two VIC8250 boards on a common VICbus. The Monitoring crate contains the hardware of a fast local data acquisition system for the L2TT. Its specification and usage are further described in Sec. 6.

## 5.2 Signal flow

The internal signal flow of the L2TT is depicted in Fig. 5. The L2busses (Sec. 3.3) enter the ACQ cards, which contain the event data during the analysis of the event. We call the principal 10 ACQ cards BT-ACQ cards, as they are directly associated with the BT-Quickbusses and hold data according to the calorimeter geometrical partitions in  $\theta$  and  $\phi$ . The GLOB-ACQ card was initially foreseen as a “wild card” which can correlate data from different detectors, which cannot be correlated otherwise due to the coverage of limited regions of the other ACQ cards. The ACQ cards are reset and cleared at L1keep. During phases 1 and 2 (cf. Sec. 4), the Command-Decision card sends the different analysis conditions, i.e. the event mapping condition and the projection selection at the maximum rate of one condition per HClk. For each mapping condition, each of the BT-ACQ cards sends the corresponding elements of the  $16 \times 16$  Boolean matrix to the TOP card. The latter makes an analysis of the matrix for each condition and yields the following quantities (cf. Fig 5):

- the number of small clusters ( $\nu$ , 3 bits),
- their proximity (Prox, 1 bit),
- the presence of big cluster(s) (Big, 1 bit),
- the projections of the matrix on the  $\Theta$  and  $\Phi$  axis, where granularities are reduced from sixteen to eight ( $2 \times 8$  bits),

defined precisely in Subsection 5.4.2. This 21 bit word is sent back to the Command-Decision card after a cycle time of 4 HClk. The GLOB-ACQ card in turn makes a direct analysis of its specific data extracted for each projection and sends a 32 bit wide result directly to the Command-Decision card.

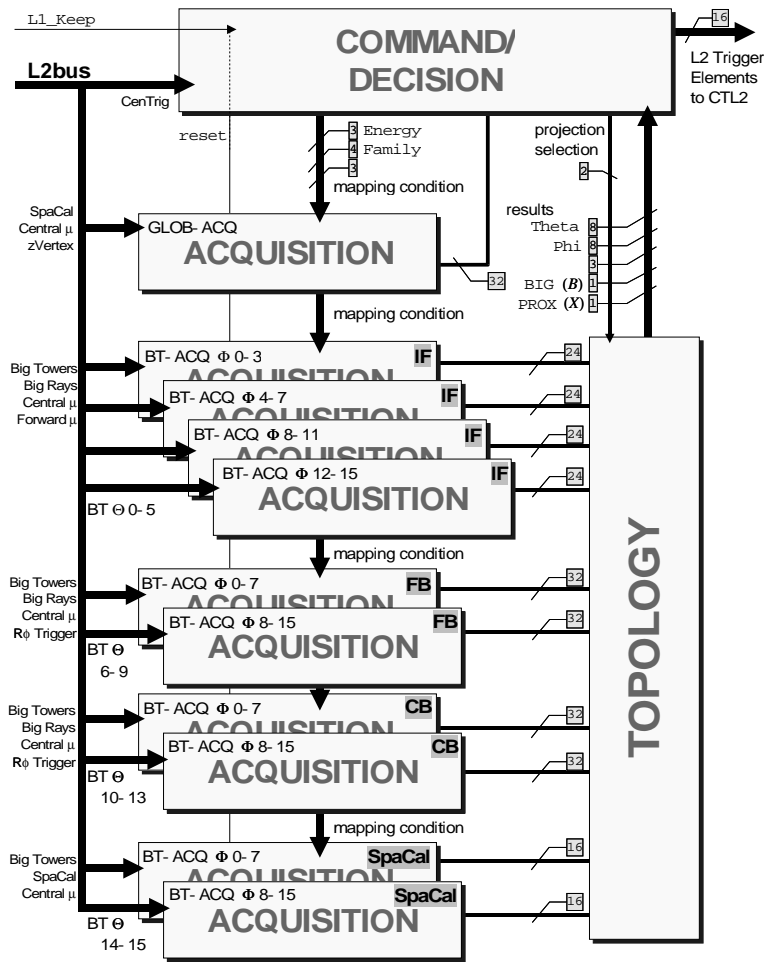


Fig. 5. Overview of the internal signal flow in the L2TT system: The signals from the L2busses enter the BT-ACQ cards which send the contents of the  $\Phi - \Theta$  matrix to the TOP card with exception of the GLOB-ACQ card. The result output of the TOP card is sent to the Command-Decision card which makes up the 16-bit decision (L2TT elements) from the extracted values and sends it to the CTL2. The ACQ and TOP cards are steered for the analysis from the Command-Decision card by the projection selection and the mapping condition. The bus widths of the internal connections are indicated in the little squared tags.

For each condition, the Command-Decision card extracts topological descriptors ( $\nu$ , Big, Prox) from the information sent by the TOP card and the corresponding data generated by the GLOB-ACQ card. Then it initiates further projection sequences (in phase 1) or increments the distance counters (in phase 2) as described in Sec. 4. After all analyses have been finished, the Command-Decision card sends the 16 bit decision word, containing one bit per L2TT trigger element, to the CTL2. The Command-Decision card contains two sets of FIFOs, which record the dataflow of analysis parameters and results at different steps of the algorithm. Every FIFO is mirrored, in order to permit independent readout by the central H1 DAQ on one hand and the local L2TT DAQ (Sec. 6.2) on the other. The remainder of this chapter will

describe the details of the three card models of the L2TT system in the order of the signal flow.

### 5.3 Acquisition cards (ACQ)

Each ACQ card stores the L2 data from the L2busses during one event and transforms those into digestible data for the TOP and Command-Decision cards. This task is accomplished by several complex, configurable input and output functions. The Command-Decision card itself determines how these output data are computed by sending the mapping conditions. Speaking in our example of Sec. 4 they are used to build up the drafts towers in Fig. 3 electronically in our hardware.

Each ACQ card is connected to the L2busses which carry the data input of each event at phase 0. During phases 1 and 2 the card sends one 32-bit output per HClk. Each card has its own specification (cf. the five groups of cards in Fig. 5) which depends on four ALTERA PLDs. The printed board design of all ACQ cards is however identical and each board derives its actual purpose by decoding three hardwired, position dependent lines of the private bus (J3) on the backplane and through the contents of RAMs, which are filled during the download procedure.

The calorimeter energy information is transmitted to the L2 systems on 10 different Quickbusses as described above (Sec. 3.3, Fig. 2). The BT-ACQ cards are associated with a specific geometrical zone of the  $\Theta$ - $\Phi$  plane in parallel to the partitions of the Quickbusses and share the treatment of information from different subdetectors as detailed on the left border of the global view (Fig. 5).

Fig. 6 shows the block diagram of an ACQ card. It has the input signals “Reset”, “Read time count”, “L2bus”, “spatial position bits” and the mapping condition, which is received as 10-bit word from the Command-Decision card. During phase 0 the information from the L2busses is written to the storage cells of the board: four “32 bit Registers” with “Filter & map” circuits (Altera PLDs) for the tracking data and eight “Calo” circuits for the calorimeter data. All the registers are latched after the acquisition time, and the 32-bit output will be used during phases 1 and 2. Only 24 bits of the ACQ cards for the IF partitions are used in reality, as these partitions cover only one fourth (4  $\Theta$ -indices) of 6  $\Phi$ -indices, whereas CB and FB type cards cover  $4 \times 8$  ( $\Phi \times \Theta$ )-indices each (cf. Tab. 1). Each of the 32 bits is the logical conjunction of 4 bits from the tROM system and one corresponding bit from the cROM. In the picture of Fig. 3 each bit indicates, if a given cell is occupied or not. The output of the ACQ card is sent to the TOP card from the BT-ACQ cards or

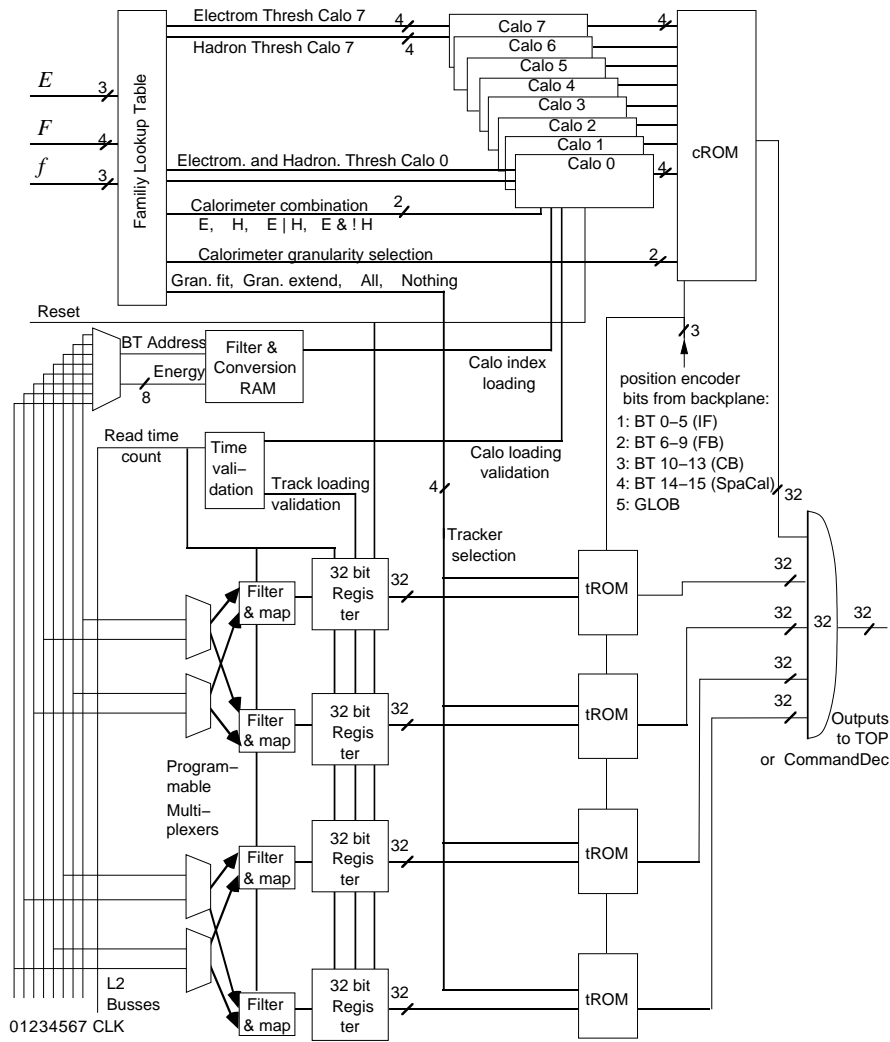


Fig. 6. ACQ card: Signal flow is from the left to the right. The components in the upper part of the drawing treat the calorimeter data and those of the lower part the tracking data. In the upper left corner of the drawing is a special 1K RAM (Family Lookup Table) which translates the 10-bit condition from the Command-Decision card into the 72-bit controlling output for the ACQ card circuits. The connection to the L2busses is shown in the lower left part of the diagram. The bus widths are indicated by tags as in Fig. 5.

directly to the Command-Decision card in the case of the GLOB-ACQ card.

### 5.3.1 Acquisition of the L2bus information

After receiving an L1\_keep signal, the ACQ cards run in acquisition mode during phase 0. All registers of the ACQ cards are first reset. The input signal "Read time count" is a number which is incremented by the L2bus clock. Data which are not zero-suppressed (like the tracking data) can be indexed and decoded through this clock counter. It is also used by the "Time validation"

circuit to eventually forbid any further acquisition by the tracker registers ("Track loading validation" signal) and to allow the calorimeter registers to acquire information ("Calo loading validation").

The five "Programmable Multiplexers" can connect one bus out of the L2busses within certain limits as seen in Fig. 6 to each tracker register, and one to the calorimeter system. They are programmed at load time of the steering file (cf. Sec. 6.1). One ACQ card is hence connected to up to 5 L2busses: one for each tracker register and one for the calorimeter data. The data of each L2bus can be dispatched into two out of the eight tracker registers.

The "Filter & map" circuit in the tracker part is programmable and can force the state of a data bit regardless of the actual data content, thus discarding temporarily noisy or dead channels of any tracking device.

The information stored in each calorimeter cell circuit is a 4 bit value of energy indices which are computed through the circuit "Filter & Conversion RAM" for the electromagnetic and hadronic BTs. The conversion of the 8-bit energy value to the 3-bit energy index is very flexible and any lookup table may be used, whereas it only makes sense to use monotonously rising functions.

### 5.3.2 *Treatment of the information*

After the end of the transmission from the L2busses, the registers are latched and the Command-Decision card sends the different mapping conditions at HClk rate during phase 1 and 2. The condition is received by each ACQ card as the address of a special 1KB RAM, the Family Lookup Table. The output of this table is detailed in Fig. 6. It translates the mapping condition for the circuits on board into precise individual instructions how to determine, if a  $\Theta$ - $\Phi$  cell is empty or full. The universality of the tROMs and cROMs is possible because they allow five different addressing modes, which depend only on the encoded type of the ACQ card.

For the calorimeter, the "Calo" circuits compare the energy indices of electromagnetic and hadronic BTs stored in the corresponding cells with hadronic and electromagnetic thresholds determined by the RAM. The hadronic and electromagnetic BTs above a requested threshold are mixed by a logical gate array. The result depends on the value of "calorimeter combination" which gives four possibilities to combine the BT energy from the electromagnetic and hadronic part of the calorimeter, e. g. E&!H, a BT cell with an electromagnetic energy above an electromagnetic energy threshold (Electrom Thresh) and no hadronic energy above a hadronic energy threshold (Hadron Thresh).

The  $\Phi$  granularity varies from 4 to 32 for different  $\Theta$ -indices (cf. Tab. 1). The cROMs convert these variable resolution data to a homogeneous 16-bit input

for each  $\Theta$  bin into the TOP card, depending on the value of the “calorimeter granularity selection” from the Family Lookup Table.

A similar treatment is made with the tracker information, evidently without the involvement of any threshold. The tROM systems play the same role as the cROMs for the calorimeter data and perform the  $\Phi$  granularity conversion according to the “tracker selection” given by the Family Lookup Table.

#### 5.4 Topology card (TOP)

The TOP card performs a topological analysis of  $16 \times 16$  two-dimensional Boolean patterns. This analysis is essentially based on cluster finding in this  $\Theta$ - $\Phi$  plane. We define the following terms:

- A *cluster* is a set of adjacent activated cells with a common boundary or a common corner.
- A *small cluster* is a cluster which can be included in a  $2 \times 2$  square.
- A *big cluster* is a cluster which cannot be included in a  $2 \times 2$  square.
- Two small clusters are said to be *well separated* if a zone of empty cells, at least two lines (in  $\Theta$ ) or two columns (in  $\Phi$ ) wide, exists between them. The circuits work in negative logic for this property and set a *proximity* bit (Prox), if separation cannot be established in the analysis.

##### 5.4.1 Elementary circuit and ASIC

The recognition of clusters and their properties on the  $16 \times 16$  Boolean matrix is implemented by 256 elementary circuits with one elementary circuit attributed to each cell, its *reference position*, of the matrix. The electronic function of the elementary circuit is depicted in Fig. 7. It generates three signals associated to the reference position b3. The presence of a small cluster within the  $2 \times 2$  square (b2,b3,c2,c3) is indicated by the “clust” signal, if its upper left corner coincides with b3, which gives 10 possibilities (◻, ◻, ◻, ◻, ◻, ◻, ◻, ◻, ◻, ◻). The five remaining small clusters which could also be included in the  $2 \times 2$  square (◻, ◻, ◻, ◻, ◻) are redundant, because they will already be found by the elementary circuits for the neighbouring reference positions. The  $3 \times 3$  reference square for the identification of a *big* cluster is centered around the reference position b3. The same  $3 \times 3$  square serves as a reference for the detection of the separation of any two clusters whose borders lie on the outer columns or rows, and who may have a connecting point inside the square. By covering the whole  $\Theta$ - $\Phi$  matrix with elementary cells for each cell, any possible local occurrence of the three properties will be detected. The output signals of each local cell are the presence of a small cluster (clust), the presence of a big cluster (big) and the proximity of two small clusters (prox).

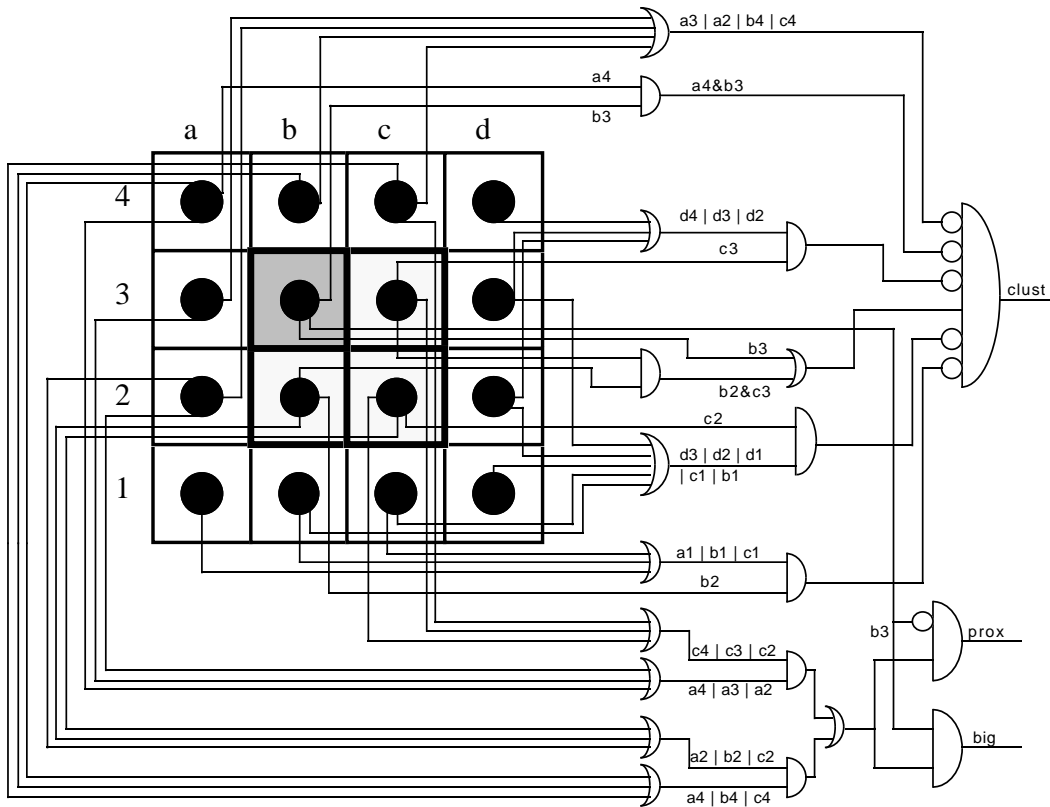


Fig. 7. Elementary circuit for clustering: The reference square (b-c;2-3) for the small cluster and the surrounding empty cells can be contained in the depicted 4×4 submatrix. The circuit detects the presence of a *small* cluster with its upper left corner in reference position b3 as described in the text. The same reference position serves furthermore as the pivot point for the detection of *big* clusters in the square (a-c;1-3), as well as for the separation of two small clusters which could potentially join in b3.

An application specific integrated circuit (ASIC), housing 32 of these elementary circuits, has been developed in our labs. It carries out the cluster finding for two contiguous  $\Phi$  sectors using inputs from five adjacent  $\Phi$  sectors over the whole  $\Theta$  range. The eight ASICs with  $5 \times 16$   $\Theta$ - $\Phi$  coverage cover the entire  $\Phi$ - $\Theta$  matrix according to the overlap scheme listed in Tab. 4.

Table 4

ASIC overlap scheme. One ASIC accomplishes the clustering for two  $\Phi$ -indices over the whole  $\Theta$ -range. Each circuit needs the input from five contiguous  $\Phi$ -columns.

ASIC	$\Phi$ -indices	ASIC	$\Phi$ -indices
0	15...3	4	7...11
1	1...5	5	9...13
2	3...7	6	11...15
3	5...9	7	13...1

Each ASIC delivers 13 output bits:

- The number of small clusters which have been found by the 32 elementary circuits. This number saturates at 7.
- A logical variable indicating the presence of at least one big cluster (local Big).
- A logical variable indicating separation of all small clusters small clusters (negative local Prox).
- The  $\Theta$  projection of the pattern which is made with a reduced granularity of 8 instead of 16. In order to obtain this reduction, it is necessary to project the output bits of four elementary circuits onto one bit. The projection method for this can be chosen among four possibilities according to the projection selection  $P$ .

#### 5.4.2 Complete Topology card

Fig. 8 shows the complete schematic drawing of the TOP card and the connections of the ASICs. This is the electrical implementation of the connectivity described in Tab. 4. The cell signals of 5 contiguous  $\Phi$  sectors (80 bits) from the ACQ cards and the 2-bit projection selection from the Command-Decision card are the input to each ASIC. The Topology card delivers 21 output bits as follows:

- The total number of small clusters which is computed by adding the numbers given by the eight ASICs. It saturates at 7 as well.
- The Prox and Big signals which are the boolean disjunction of the corresponding signals from the eight ASICs.
- $\Theta$  projection pattern which is the boolean disjunction of the 8 bit  $\Theta$  projections from the ASICs.
- $\Phi$  projection pattern which is the boolean disjunction of the 8 bit  $\Theta$  projection from each of the eight ASICs, composed to an 8-bit-word.

#### 5.5 Command-Decision card

The Command-Decision card has two separate functions performed by two units. The **Command unit** (Sec. 5.5.2) controls and synchronizes all operations within the complete crate according to the phases 1–3 described in Sec. 4. The **Decision part** (Sec. 5.5.1) uses the results of the TOP card and the GLOB-ACQ card to determine for each mapping condition a descriptive class code (explained below) and a distance result, which is summed up individually for each trigger element in the Command unit. The Command unit makes its final decision on each trigger element by comparing each of these sums to a threshold value. The activities on this card are triggered by an L1\_keep signal and a signal which indicates the end of the L2bus data acquisi-

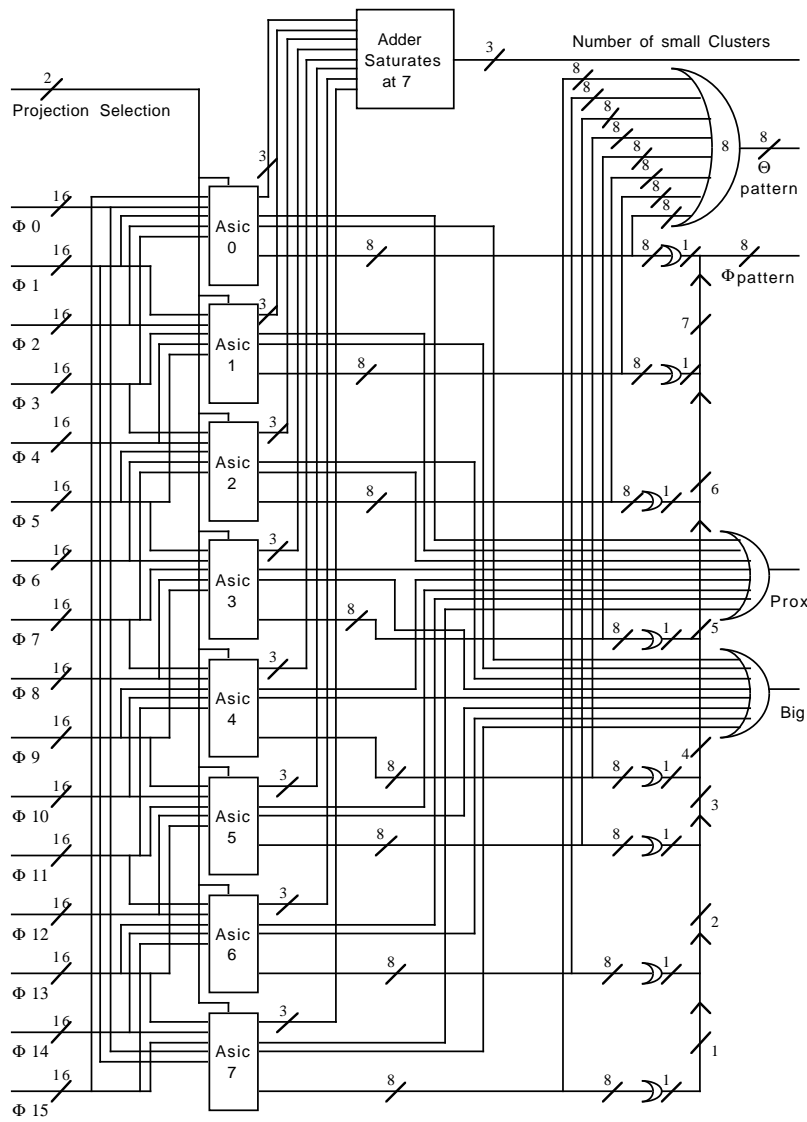


Fig. 8. Topology card: Signal flow on this picture goes strictly from the left to the right and bus widths are indicated by small numbers at slashes as introduced in previous figures. The 80 bits from 5 adjacent  $\Phi$  sectors and 2 bits for the projection selection are connected to each ASIC. One ASIC delivers 13 output bits which represent the  $\Theta$  projection pattern (8 bits), the number of small clusters (3 bits) and 2 logical variables (local Prox and Big). The outputs from all ASICs are resumed to 21 bits for the entire  $\Phi$ - $\Theta$  matrix, as explained in text (cf. Sec. 5.4.2).

tion in the ACQ cards. The final 16-bit decision in form of trigger elements is also sent from this board. The two units are described in detail in the following two subsections.

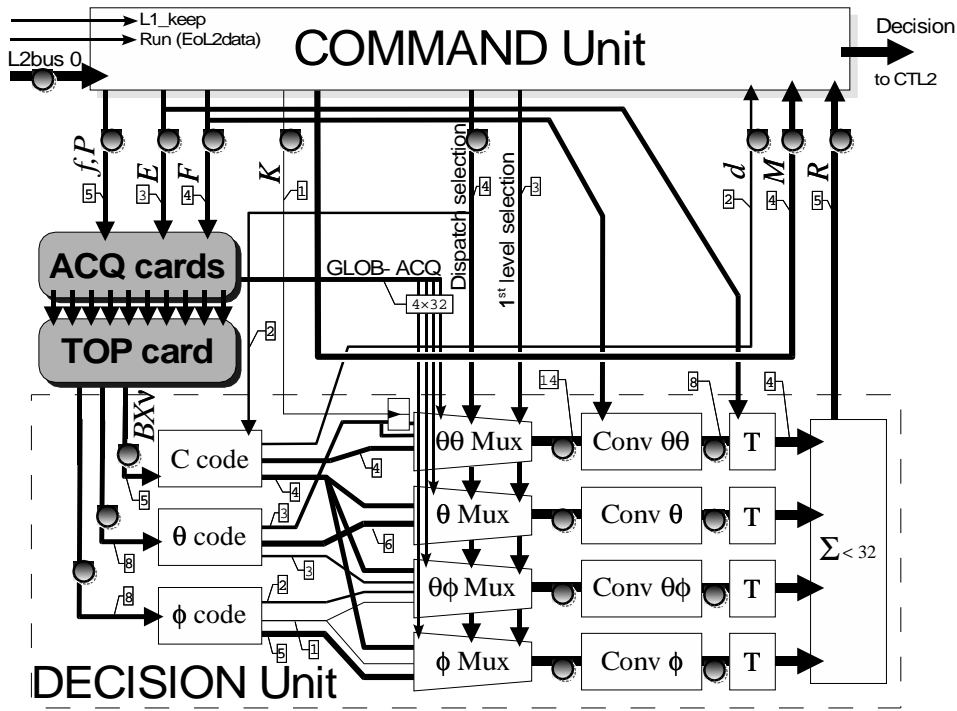


Fig. 9. Command-Decision card, and the Decision part in particular: The external parts, ACQ-cards and TOP-card, are represented as shaded blocks. The Command part controls this periphery as well as the Decision part in the lower part of the drawing by the numerous control signals explained in the text in order to generate various projections of the event. As a result of these projection requests, the Decision part produces the  $d$  (description) value and the  $R$  (result) value after passing the TOP/ACQ results through a recoding stage and four almost identical chains of correlation logic as described in the text. Monitoring FIFOs, which register all data passing during the analysis of an event, are indicated by the shaded circles. The input and output signals into and from the L2TT system are connected to the Command part in the upper part of the figure.

### 5.5.1 Decision part

The details of the Decision part are presented on Fig. 9 within the context of the complete Command-Decision board. The previously described TOP and ACQ cards appear here as shaded blocks, in order to illustrate the interface. They deliver the projections on the  $\theta$  and  $\phi$  axes and the cluster descriptors  $B, X, \nu$  (for Big, Prox and number of small clusters) at the input of the specialized Decision network consisting of several stages of electronic memory and logic circuits. The GLOB-ACQ card delivers four 8-bit words, which enter directly the network at an intermediate stage of evaluation. For a given set of event data in the ACQ cards, the output of the TOP/ACQ group only depends on the input signals for the mapping conditions, which are generated by the Command part. It can be simulated on board by a special SIM-RAM for complete simulation of the apparatus whereby only the Command-Decision card is used.

The outputs from the TOP card are reduced in three EPROMs labelled “ $\Theta$ -code”, “ $\Phi$ -code” and “C-code” by converting this information into a number of  $\Theta$ -,  $\Phi$ -, and cluster multiplicity codes [25]. A rough summary of the topological analysis is generated in this first step of data treatment into a 2-bit *class code*  $d$ , describing four types of event projection results:

- $d=0$  projections with *an empty topology*,  
no signals on the  $16 \times 16$  Boolean matrix have been found,
- $d=1$  projections with *a trivial topology*,  
having only one small cluster and no big cluster, and
- $d=2$  projections with *a non-trivial topology*,  
with more than one small cluster and no big cluster or
- $d=3$  projections with *a non-trivial topology and at least one big cluster*.

This  $d$  value is input to the Command circuit and taken into account in phase 1 for the rapid evaluation of the projections.

Further outputs of the code-EPROMS serve as inputs to four almost identical chains of correlation logic with a multiplexer-PLD, conversion-RAM and threshold-ROM each. The output of the threshold-ROMs is added to a result value, which is sent back to the Command part and saturates at 31. The four chains are labelled  $\phi$ ,  $\theta$ ,  $\theta\phi$  and  $\theta\theta$ . They differ by their input data, in the way that six bits out of fourteen receive different data from the code-EPROMS, and the eight bits from the GLOB-ACQ are possibly different for each chain. The different data from the code-EPROMS enable the circuitry to:

- $\phi$  evaluate the pattern of the  $\phi$  projection,
- $\theta$  evaluate the pattern of the  $\theta$  projection,
- $\theta\phi$  correlate the patterns of the  $\phi$  and  $\theta$  projection and evaluate the result,
- $\theta\theta$  correlate the pattern of the  $\theta$  projections for two different mapping conditions and evaluate this result.

The double- $\theta$  correlation mentioned at last is implemented by means of a D-FlipFlop, which stores the (reduced) 3-bit  $\theta$ -code from any mapping condition as soon as the Command unit sets the “keep” signal ( $K$ ) active. The simultaneous presentation of two reduced  $\theta$ -codes from two distinct mapping conditions to the multiplexer input becomes feasible in this way.

Each multiplexer outputs 14 bits, which represent the compressed information from topological analysis, global L1 trigger conditions coming from the GLOB-ACQ card and signals from the Command unit (1st level selection and dispatch selection). The dispatch selection signal chooses between different codings. These 14 bits together with the 4-bit family number, coding the selected input correlation, form the inputs to Conversion RAMs, which contain an 8-bit recipe for computing (the contribution to) the distance to background. The circuits labelled “T” are EPROMs, which convert this 8-bit value from

the Conversion RAMs into a 4-bit value of the distance to the background, taking into account the 3-bit energy index. The adder circuit sums up the distances (saturating at 31) and the final output result ( $R$ ), representing the distance to background contribution, is sent to the Command part.

Pairs of Monitoring FIFOs at several places record the history of signals during the analysis of an event (cf. Fig. 9). One set of (analysis) FIFOs is reset active at L1\_keep and can be read by the central data acquisition system at the rhythm of H1 Central DAQ data taking. A second, parallel, set of (monitoring) FIFOs is read out by the local L2TT DAQ system (Sec. 6.2), which must authorize their clearance and reactivation. This prevents mixing of events as the monitoring system is not synchronized with the acquisition system and must not interfere with the treatment of new incoming events. The FIFOs are clocked by HClk, thus recording an exact image of the analysis in phase 1 and 2. The drawing shows the monitoring FIFOs as shaded circles on the signal lines.

### 5.5.2 Command part

Beside the correct processing of all mapping condition requests and the returning results as a consequence of that, according to the general L2TT algorithm, the Command part is also responsible for the speed optimization of the request-response sequence. The propagation delay of the signals in the TOP/ACQ cards and the Decision part is not negligible with 3–4 HClk. Hence the transmission of the mapping conditions and the reception of the results are operated in a request-result protocol, controlled by a Digital Signal Processor (DSP) in the Command part. Optimal use of the processing time within the given time constraints has been achieved by decoupling the transmission-reception actions from the evaluation procedure in the DSP.

Special care had to be taken for the synchronization of signals within the peripheral circuitry. In spite of the very different signal paths (cf. Fig. 9), the mapping conditions (like  $E, F, f, P$ ) need to arrive in the Command part simultaneously with the  $d$  or  $R$  result, and even the auxiliary “machine number” data  $M$ . Some signals (like the energy index  $E$ ) are even inserted at two different stages of the process path. Again the HClk frequency is used here to clock the propagation of the signals in the processing blocks by means of intermediate latch registers and adjustable delay loops for the latency fine tuning.

A 32 bit/32 ns instruction cycle microprocessor (Analog Devices DSP 21020) has been chosen for the function of the central Command CPU, which is illustrated in Fig. 10. It has two independent data busses for accessing data memory (DM) and program memory (PM). This allows the simultaneous ac-

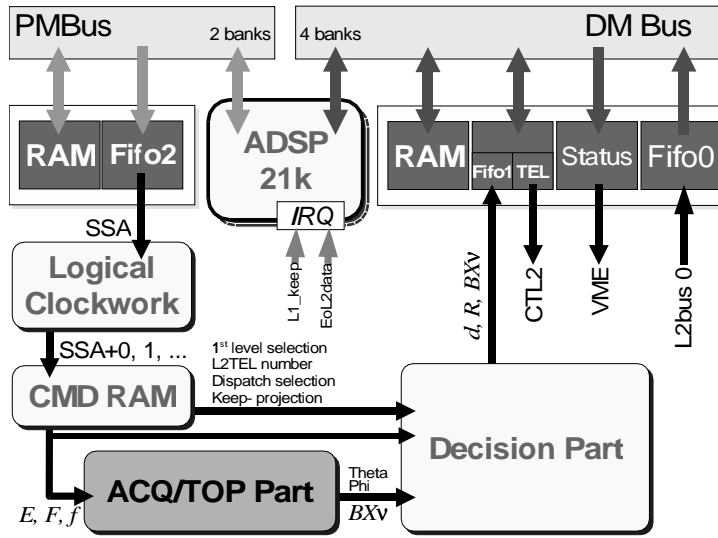


Fig. 10. Processor communication architecture of the Command-Decision card: The DSP uses its two peripheral buses (DM for data memory and PM for program memory) also for optimizing communication with the L2TT specific hardware interfaces. Inputs (Fifo0, Fifo1) and output (Fifo2) datastreams are buffered and thus desynchronized from the internal DSP program. The DSP sees the L2TT hardware as a circuit with (on this figure) counter-clockwise dataflow. From the Fifo2, projection sequences are launched with the logical clockwork through the command (CMD) RAM. It is possible to simulate the passage through the TOP and ACQ cards entirely by an on-board simulation (SIM) RAM. The output of the Decision part is buffered in Fifo1, from where data are read back into the DSP.

cess of two peripheral devices like memories; algebraic operations inside the DSP can be performed in parallel. The DSP is interfaced to the rest of the system through FIFOs capable of zero dead time accesses.

The start condition of the system is the L1\_keep signal. At this time, the DSP enters an initialization phase parallel to the collection of subdetector data in the ACQ boards. The duration of this phase 0 is approximately  $6 \mu s$ . At its end, the “End of L2 data” signal informs the DSP that the computing phase can be launched. Then the DSP sends the *Sequence Start Address* (SSA) through the PM bus to Fifo2. The logical clockwork sequencer detects data in this Fifo and begins incrementing the address values of the CMD-RAM from SSA up to an END condition. This END condition is contained in CMD-RAM data and is sent back to the clockwork as soon as one of the END-addresses appears. The sequencer then looks for a new Fifo2 word or just stops, if it is empty. The CMD-RAM sends the sequence of mapping conditions to the Decision part and the ACQ/TOP cards. All results coming back from there are collected in Fifo1, which is read out by DSP via the DM bus.

Thus, the four phases for the event analysis, which have been defined in Sec. 4, are translated into the CPU algorithm as follows:

- Phase 0: The DSP initializes the registers and verifies that no time-out occurs. It computes the L1 trigger selection, while the ACQ cards receive the L2 data for the event. The initial SSA is sent to Fifo2.
- Phase 1 splits into two parallel tasks for data input and output:
  - Phase 1.1: The sequence of 8 words per first phase key correlation with the decreasing energy indices is sent. This sequence is the same for all events.
  - Phase 1.2: During analysis of the first phase results, the DSP reads the results as the class code  $d$  (cf. Sec. 5.5.1) from Fifo1, determines the primary and secondary energy indices and computes the SSAs which are to be used in the next phase.
- Phase 2: The distance-to-background contributions ( $R$ ) from the Decision part are collected in Fifo1. The DSP reads the  $R$  value and the trigger element number  $M$  from Fifo1. For each Fifo1 word it adds  $R$  to the content of one of the 16 trigger element registers in the memory.
- Phase 3: The DSP compares the contents of the different trigger element memories with the corresponding distance thresholds and builds the 16-bit trigger element word. This word is sent to CTL2 and the transfers of the contents of monitoring FIFOs to Monitor card is initialized.

The DSP program is written in assembler language. The proprietary programming tools also contain advanced simulation possibilities. The choice of both the DSP processor and the assembler language is due to the fact that the decision time has to be perfectly deterministic. The program contains the different strategies that have to be performed for building the final decision. It is stored in a RAM accessible through VME and thus can be modified on request.

## 6 Control and monitoring

### 6.1 *Steering file*

The design of the L2TT hardware makes the programming of the trigger behaviour highly flexible. The relevant programmable parts are of two different types:

- RAMs in the different cards, which can be rapidly loaded online, and
- programmable ALTERA PLDs (cf. Sec. 5.3), (E)PROMs and PALs, (cf. Secs. 5.3.2, 5.5.1), which have to be taken off the circuit boards to be re-programmed.

The setup of these parts is described in ASCII format in a single *steering file*, which is also written to the H1 main database NDB in parallel to its

usage on a per run<sup>5</sup> basis [26]. The loading of the complete trigger takes not more than some minutes. Among others the steering file contains the following information:

- hardware version identifier, including a description of the PLD, EPROM and PAL configuration,
- information allowing the programming of the PQZPbus and Quickbus Receivers, such as number of words transmitted by the different subdetectors connected to the different ports and the timing of the transmission of this information on the L2bus,
- eventually dead or noisy tracker bits which must be ignored for every event,
- calorimeter thresholds applied in different families,
- the specification of the different families,
- the sequence of the mapping conditions,
- the distance thresholds applied to each of the 16 trigger elements,
- the contents of the Conv-RAMs (4×1 MB, cf. Sec. 5.5.1) in compressed format.

## 6.2 Local Data Acquisition

An L2TT internal local DAQ system (Monitoring crate, Fig. 4 and Sec. 5.1) allows the recording of event samples which are being examined by the L2TT. The advantage with respect to the central DAQ through the Central Trigger is that it can record also those events which are rejected by the L2 triggers and therefore not read out centrally. This feature allows non-interfering diagnostics of trigger behaviour during normal data taking. At each stage of data computing within the hardware of the Command-Decision card, the flowing information is stored in 10 Monitoring FIFOs (cf. Sec. 5.5.1 and Fig. 9). After having sent the decision to the Central Trigger, the DSP allows the transmission of all those FIFO contents to the local DAQ system.

The local DAQ process runs on the 68040 CPU [27] of a Fast Intelligent Controller (FIC8234) [28] under the real time operating system OS/9 by Microware [29]. The Monitoring crate contains two VICbus nodes (VIC8250). The VIC connection to the Central Trigger is used for the reception of run information. The second VIC connection ends in a MAC7212 card in the Control Mac and allows data acquisition rates of up to 8 Mbytes/s.

The Monitoring card initiates the transmission of the contents of the 10 monitoring FIFOs of the Command-Decision card. They are received through a custom 16-bit differential ECL [20] cable (which is compatible with the PQZPbus) and stored in an internal 32×64 Kb FIFO buffer. The transmission is

---

<sup>5</sup> A run in H1 is a data sample collected with stable trigger conditions.

driven by the Command-Decision card. The Monitoring card makes sure that it receives complete events, whereas the Command-Decision card doesn't erase its FIFOs as long as an event is not completely transmitted. The FIFO buffer is later on emptied by the FIC in 32-bit words through the VME bus (A32D32 mode).

A graphical user interface (GUI) for the steering of the monitoring software in the FIC and displaying L2TT data is running on a Mac. The main task of the OS/9 system is to readout the contents of the Monitoring card, format them and place them into a multievent buffer, managed by a software package from CERN [30]. This event manager works in a producer-consumer scheme and allows up to 64 parallel independent OS/9 processes to read events from the buffer and to perform on-line checks of the L2TT [31]. The control of the monitoring software and the survey of results of monitoring processes and the readout status of the Monitoring card is done on the Mac by the L2TTMon application [32], based on the GUI. A dedicated server-client protocol for the communication between this application and the monitoring processes on OS/9 uses the VICbus and in particular the FIC8234 internal FIFO mechanisms. The Mac graphics library TMacLib [33] has been used for the GUI programming. The monitoring processes can also be prepared and controlled from the OS/9 commandline shell without any connection to the Mac. The most common process is the fast data storing into a local OS/9 disk file, with the possibility of a preselection based on the event content. This file, called *monitor file*, can be used later on for the development of trigger strategies as described in Sec. 6.5.

### 6.3 Simulation of the trigger

A complete simulation program of the L2TT apparatus has been developed. The simulation code uses the same information as the L2TT hardware and goes through the same steps of the analysis as in the hardware leading to the final decision. It is used mainly for two purposes: Monte-Carlo simulation and verification of the correct function of the hardware during construction or datataking, which is part of the monitoring as explained in the following subsection.

The L2TT simulation library is part of the official H1 simulation chain. It is run dependent through the steering files, which are stored in the H1 main database (cf. Sec. 6.1).

Different software tools were used to test the hardware during construction as well as during data taking. They are installed either on the Mac connected to the hardware system, or in the H1 offline analysis environment and make use of the simulation program. These tools allowed debugging of the hardware during the initial tests and are used for loading the steering file, testing of the apparatus by playback of a sample of selected events and regular tests on the events written to tape.

**Hardware tests** A special program which simulates the different cards has been installed on the Mac. At the time of the construction this program was oriented towards hardware debugging and was modified later on to allow easy loading of the steering file after power/apparatus failures or an installation of new strategies. This program also allows a rather complete test of the hardware with a sample of chosen events. The events are processed by the simulation program which writes a file containing the inputs, the decision word which corresponds to the inputs, and also the decision history as it is written in the FIFOs of the Command-Decision card. The program reads this file, writes the inputs into the PQZP and Quickbus Receiver cards, simulates the L1\_keep signal through the Spy (cf. 3.3) card, reads the online FIFOs, and compares their contents to the content computed by the simulation program. An event rate of 10 Hz was achieved in this playback mode. The speed is limited by VME reading and CPU speed of the Mac. It allowed the complete apparatus to be tested in all aspects except under high rates. This tool turned out to be very useful as a last verification when installing a new strategy, and when a malfunction was suspected.

**Offline tests** A daily test is performed on about 60,000 fully reconstructed events containing all detector data including the online result of the L2TT. The testing program uses the simulation program to compute the L2TT decision from the inputs and compares both results. No discrepancy between the online result and the result of the simulation program is allowed. This test is less complete than the playback test mentioned earlier, as it does not compare the simulated and actual decision histories because the FIFO contents are not stored on tapes. But it can reveal malfunction of the apparatus and check the coherence of the inputs.

In order to establish a steering file with selection criteria for a new analysis channel, we use both the physical event sample and background data consisting in an event sample which contributes to the defined physics channel. We obtain the latter by capturing L1 triggered (not necessarily L2-kept) events at a high rate during data taking through the local DAQ system described in Sec. 6.2. By analyzing these background monitor files we can study the rejection and acceptance efficiencies for signal and background and tune cut values. Once a newly developed strategy is used during data taking, its steering file is stored in the H1 database [26].

## 7 Examples of the trigger applications and performance

The L2TT generates up to 16 trigger elements. An overview of the most relevant setups for these elements during the years 1995–2000 is presented in Tab. 5. The subdetectors used in the selection criteria for a given trigger el-

Table 5

Overview of the installed L2TT elements. The rate reductions (subtrigger specific rejection factors of L2, L2 output rate divided by L1 output rate) for a given physics process described in the first column, are displayed in the third column. The second column contains the subdetectors which are used in the respective L2TT analyses.

physics process	used subdetectors	rejection factors
DIS NC (5 L2TT elements)	SpaCal	1.5 – 9
QED Compton scattering [34]	SpaCal	20
beam-gas pattern (2 L2TT elements) [35]	LAr	†
$ep \rightarrow ep + (J/\psi \text{ or } \Upsilon) \rightarrow e^+e^-$ [25]	LAr	15
multimuon cosmic events	central $\mu$	20
Deeply Virtual Compton Scattering	LAr, SpaCal	15
DIS NC very high $Q^2$	LAr	2000
* $\gamma p \rightarrow b\bar{b} + X, b/\bar{b} \rightarrow \mu\nu + \text{jet}$	central $\mu$ , CJC, LAr	3.5
* $\gamma p \rightarrow X + J/\psi, J/\psi \rightarrow e^+e^-$ [35]	LAr, MWPC, CJC	3.5
Deeply Virtual Compton Scattering	LAr	5
* DIS CC high $Q^2$ [36]	LAr	40

\*Detailed descriptions given in text.

†Not used as independent L2 condition.

ement and the obtained trigger rate reduction, i. e. the ratio of all events accepted by the L1 conditions over the events accepted by the L1 and — in addition — the L2TT conditions, are listed there. The rate reduction factors

met the values required for the desired physics processes. One trigger element designed to select DIS NC events with very high  $Q^2$  value was used as a security for the high  $Q^2$  L1 subtrigger, which was not prescaled in any phase. In case of a necessary prescale at increasing luminosity (and therefore background) rates, it could have been seconded by this associated L2TT element.

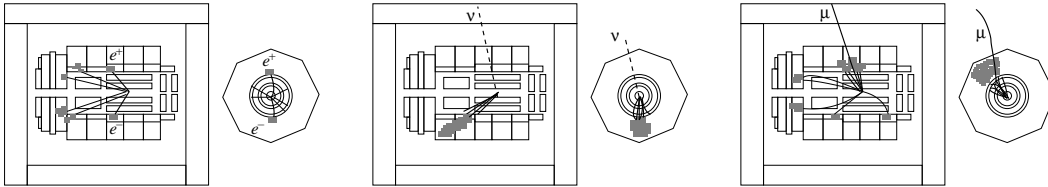


Fig. 11. Illustration of the three selected cases of Tab. 5, which are explained in detail in Sec. 7.1–Sec. 7.3: The side view, analogous to Fig. 1, with simplified schematic event signatures for each case is completed by a radial view of the central detectors around the interaction point.

Three examples for the applications of the L2TT are briefly described in the following subsections to demonstrate trigger possibilities. Fig. 11 illustrates these selected cases as seen in the H1 detector: Inelastic  $J/\psi$  production (with electronic decay), charged current scattering and open  $b$  quark production (with muonic decay). In all these examples the trigger conditions used to extract the signal are confronted to the characteristic criteria for the background rejection. In the triggering of  $J/\psi$  mesons decaying into an  $e^+e^-$  pair the main effort is put on lepton identification by their energy (electromagnetic  $E_{\text{elm}}$  or hadronic  $E_{\text{had}}$ ) deposits in the LAr calorimeter. The selection of events from weak charged current processes exploits the clear signature of the produced jet and the missing energy in these events. Finally, in the example of triggering on events containing  $b$  hadrons the expected topology is recognized by the identification of a muon within a jet from the hadronization of the  $b$  decay, regardless of the rest of the event signature.

### 7.1 L2TT element for inelastically produced $J/\psi$ mesons

The L2TT element that allows the selection of  $J/\psi \rightarrow e^+e^-$  events from inelastic photoproduction at HERA has been installed at the end of the 1997 data taking. Triggering of low energy (1–2 GeV) electrons from  $J/\psi$  decays in difficult background conditions at HERA in the L1 trigger is based on the combination of the information from the LAr calorimeter and the tracking system. The main requirements of the L1 trigger are: a well defined vertex, presence of at least 3 tracks, one high momentum track and one negative track found by the DCr $\phi$  trigger and the coincidence between a LAr BT and a BR. Before the implementation of the L2TT the main L1 subtrigger for inelastically produced  $J/\psi$  in the electron decay channel, running at the rate of a few Hz, was prescaled by a factor four in order to bring the rate down

to an acceptable level. The applied strategy searches for electron candidates identified as energy deposits in the LAr calorimeter, which may be validated by a track. In addition, background rejection criteria based on the topological analysis of signals from the very forward part of the LAr calorimeter are used.

### 7.1.1 Signal selection conditions

The selection of electron candidates from the  $J/\psi$  meson decay is restricted to the central part of the LAr calorimeter. The chosen topologies are presented in Tab. 6.

Table 6

Relevant L2TT topologies for inelastic  $J/\psi$  meson production with electronic decay

detector region	central	$\Theta$ indices	6–13
signals	electromagnetic or hadronic BTs, BRs, DCr $\phi$ trigger		
chosen topologies	<ul style="list-style-type: none"> <li>• BTs with <math>E_{\text{elm}} \geq 0.5</math> GeV (<math>\Theta=6-9</math>)</li> <li>• BTs with <math>E_{\text{elm}} \geq 1.0</math> GeV (<math>\Theta=10-13</math>)</li> <li>• BTs as above, but validated by a BR and DCr<math>\phi</math> trigger signal</li> <li>• BTs with <math>E_{\text{elm}}</math> or <math>E_{\text{had}} \geq 2</math> GeV</li> <li>• number and position of small clusters</li> </ul>		

We take into account topologies with a signal from at least one electromagnetic BT with a minimum energy, depending on the  $\Theta$  index, that may be validated by a BR or the DCr $\phi$  trigger. Higher energy electrons or electrons accompanied by particles giving energy deposits in the hadronic section of the LAr calorimeter can be selected by a signal from at least one electromagnetic or hadronic BT with a minimum energy of 2 GeV. The back-to-back signature of the decay electrons from  $J/\psi$  mesons with low transverse momentum is translated into the presence of at least two small electromagnetic clusters separated by more than  $90^\circ$  in azimuthal angle  $\phi$  without any “big cluster” signal, which is necessary to accept the event.

### 7.1.2 Background rejection conditions

The proton beam induced background has been reduced by the analysis of the topological  $\phi$  pattern of the very forward BTs with  $\Theta$  indices 0 and 1. The chosen topologies are presented in Tab. 7.

Two different trigger elements enable rejection of events with background topology. The selection criteria are based on the observation that the background shows frequently a  $\phi$ -symmetric energy deposition in the forward direction, whereas for the physics sample, the energy deposited in this region by

Table 7

Relevant L2TT topologies for background rejection (for inelastic  $J/\psi$  production)

detector region	very forward	$\Theta$ indices	0,1
signals	electromagnetic or hadronic BTs		
chosen topologies	<ul style="list-style-type: none"> <li>• BTs with energy <math>\geq 1</math> GeV</li> <li>• number and position of small clusters</li> </ul>		

the proton remnant, if present, is rather asymmetric. This difference allows an effective distinction between background and signal topologies. Background free topologies are in general characterized by energy deposits in electromagnetic/hadronic BTs with  $\Theta \in \{0, 1\}$  in less than 7 octants in  $\phi$ .

### 7.1.3 Acceptance criteria and trigger efficiency

The signal pattern in the central part of the LAr calorimeter and at least one condition indicating background free topology in the very forward region must be fulfilled. Accepted events must have at least one electromagnetic BT in the central part of the LAr calorimeter and energy deposits in less than 7 octants in  $\phi$  in the very forward BTs. Fig. 12 shows the dependence of the efficiency for the  $J/\psi$  L2TT element as a function of kinematical variables for 1997 data [35].

We obtain an efficiency of about 70% on average and observe an efficiency on the level of 80% for higher  $e^+e^-$  invariant masses,  $M_{ee} > 2.8$  GeV, and about 60% at lower values. The background rejection factor for the  $J/\psi$  L2TT element is defined as the number of events accepted by the L1 subtrigger dedicated to the studied process divided by the number of events accepted by this L1 subtrigger and validated by the corresponding L2TT element. We have determined this value to be  $\sim 3.5$ , which allowed the removal of the prescale factor for this L1 subtrigger.

## 7.2 L2TT element for charged current events

The HERA collider allows the investigation of weak charged current (CC) processes in deep inelastic  $ep$  scattering at the highest center-of-mass energies ever reached [37]. The L2TT element for the selection of CC events  $ep \rightarrow \nu + X$  has been installed since the 1996 data taking campaign. Its main goal was the rejection of the high background contamination in order to run the L1 subtrigger dedicated to this process with a low prescale factor. The main L1 subtrigger associated with CC processes requires: a vertex found by the z-vertex trigger, at least three tracks in the DCr $\phi$  trigger and the coincidence between a LAr

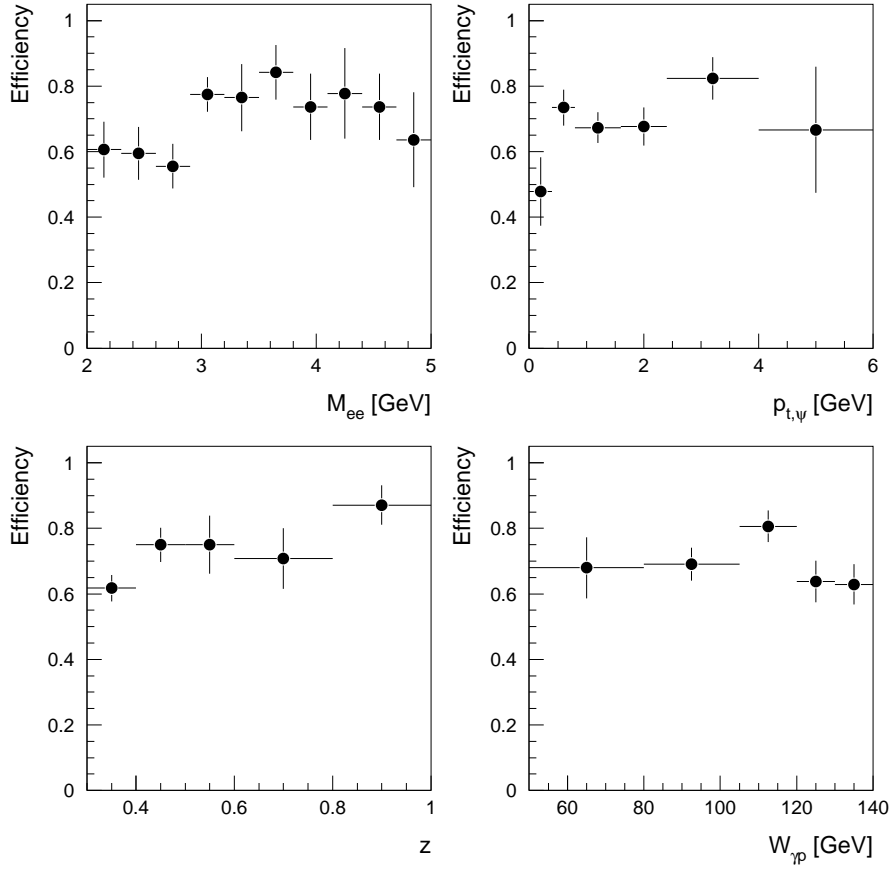


Fig. 12. Efficiency of the L2TT subtrigger for inelastic  $J/\psi$  meson production as a function of the invariant mass of the lepton pair  $M_{ee}$ , the transverse momentum  $p_{t,\psi}$  of the  $J/\psi$ , the elasticity variable  $z$ , which is the fraction of energy of the exchanged photon transferred to the  $J/\psi$  in the rest frame of the target proton, and the centre-of-mass energy of the photon-proton system  $W_{\gamma p}$ .

BT and an MWPC BR. The CC events have a very clear signature of an unbalanced hadron system with high transverse momentum, due to the undetected neutrino in the final state. This feature has also been used in the L2TT selection, which is exclusively based on the LAr calorimeter information, as shown in Tab. 8.

Table 8  
Relevant L2TT topologies for charged current events

detector region	central	$\Theta$ indices	6–13
signals	electromagnetic or hadronic BTs		
chosen topologies	<ul style="list-style-type: none"> <li>• BTs with a predefined energy threshold</li> <li>• number and position of small clusters</li> <li>• presence of a big cluster</li> </ul>		

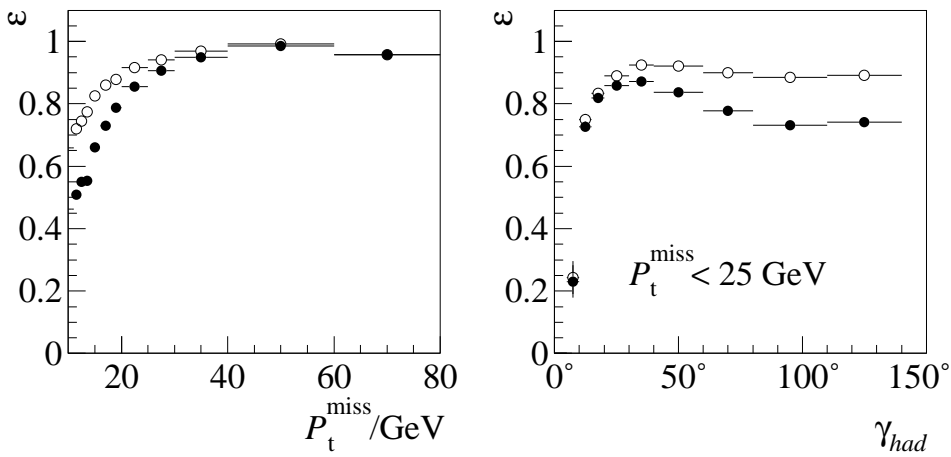


Fig. 13. Efficiency of the L1 trigger element for charged current events (circles) and after its validation by the L2TT conditions (dots) versus missing transverse momentum  $P_t^{\text{miss}}$  (left) and versus the inclusive angle of hadronic final state  $\gamma_{\text{had}}$  (right).

### 7.2.1 Acceptance criteria and trigger efficiency

The L2TT element for CC events selects a LAr BT pattern in the central detector region, which is unbalanced in  $\phi$ . Each event is attributed to one of two classes: with only one small electromagnetic/hadronic cluster or with only two small electromagnetic/hadronic clusters (cf. class code  $d$  of Sec. 5.5.1), present in the same  $\Phi$  sector or in two adjacent  $\Phi$  sectors. In both cases the cluster energy must be above 2 GeV and the absence of a big cluster is required. Accepted events must belong to at least one of these classes. The efficiency of the main L1 subtrigger for CC events is compared in Fig. 13 with its efficiency in the case of validation by the L2TT element for CC events, as a function of two variables (defined more precisely in [36]): the missing transverse momentum  $P_t^{\text{miss}}$  and the inclusive angle  $\gamma_{\text{had}}$  of the event, which indicates the direction of the jet generated from the scattered parton. Triggers were optimized to cover a maximum of the phase space for the studied process. The inefficiency introduced by the L2TT conditions is approximately 8–10% for  $P_t^{\text{miss}} < 25 \text{ GeV}$  and becomes negligible for higher  $P_t^{\text{miss}}$  values. The achieved rejection factor is about 40 and allowed us to set low prescale factors for the main L1 subtrigger associated with the CC process.

### 7.3 L2TT element for open $b$ quark production

The H1 Collaboration has observed open beauty production at HERA [38]. The production of  $b$  (or  $\bar{b}$ ) quarks is tagged by muons from the semileptonic  $b$  decays, where at least one muon is identified in the central region of the detector. The muon has to be found within a jet. The main L1 subtrigger used to select this channel requires the presence of at least one muon in the

barrel region of the central muon chambers and, in the DCr $\phi$  trigger, the presence of at least one track with  $p_t > 800$  MeV and one negative track. The rates of this L1 subtrigger have been well below 4 Hz. In order to avoid prescaling factors at expected higher luminosity, we have introduced these L2 conditions since the end of the 1997 data taking.

### 7.3.1 Signal selection conditions

The main condition of the physics selection “ $\mu$  inside a jet” imposes the kind of topology that we have to require, a coincidence between a muon signal and a “jet like” structure in the event. Such a structure could manifest itself as an energy deposit in the LAr calorimeter or/and the presence of one or several high momentum tracks seen by the DCr $\phi$  trigger. The topologies given in Tab. 9 have been chosen for the implementation.

Table 9  
Relevant L2TT topologies for open  $b$  quark production

detector region	forward and central	$\Theta$ indices	0–13
signals	electromagnetic or hadronic BTs, central muon trigger, DCr $\phi$ trigger		
chosen topologies	<ul style="list-style-type: none"> <li>• number and position of small clusters</li> <li>• presence of a Big cluster</li> <li>• forward BTs with a predefined energy threshold</li> <li>• central BTs with a predefined energy threshold</li> <li>• muon signal and its position</li> <li>• validation of the muon signal by DCr<math>\phi</math> trigger</li> <li>• validation of the muon signal by a BT with a predefined energy threshold</li> </ul>		

### 7.3.2 Background rejection conditions

Physics and background events differ significantly in the position of a muon signal in the detector. The majority of the background events has a muon in the forward barrel from upstream conversion of beam-halo protons in the accelerator. Physics data populate equally forward and central barrels. Thus we defined less restrictive selection criteria, whenever the muon is in the central barrel, as these events show less background contamination. In order to improve the reduction of the proton beam induced background, similar criteria as for the  $J/\psi$  L2TT algorithm (in Sec. 7.1.2) have been applied to this L2TT element.

### 7.3.3 Acceptance criteria and trigger efficiency

The selection conditions for accepted events are set up in a way to give preference to events with a muon signal in the central region validated by an energy deposit in the corresponding BT or DCr $\phi$  trigger signal in the same ( $\Theta$ ; $\Phi$ ) region and showing a large activity in the central region. More than 90% of the examined  $\mu$ +jet event sample events have been accepted, keeping the background rejection factor between 3 and 4 with respect to the dedicated L1 subtrigger.

### 7.4 Summary

Since the introduction of the L2TT system it has been efficiently used for selecting various physics processes from background. The topological L2 trigger of the H1 experiment generates up to 16 trigger elements. Various algorithms permitted the refinement of the L1 trigger conditions for some physics processes, thus reducing their trigger rates by applying this additional L2 condition as required while the luminosity increased by a factor 5–6 during the first period of HERA operation, conditioning significant changes of the background situation as well. A judicious choice of diverse available technologies as described in the hardware section of this article made the topological L2 trigger flexible enough to respond to different physics requirements in a changing experimental environment. Performance and reliability of the apparatus have been proven to be very good. It constitutes a fast and efficient intermediate trigger system for a high energy physics collider detector, which can inspire the design of future devices that will be used in even more challenging environments.

### Acknowledgement

This work was supported by the LAL and the IN2P3 and by the Polish State Committee for Scientific Research (grant no. 2P031/318 and SPUB/DESY/P-03/DZ 1/99). We thank the DESY directorate for the hospitality which they extend to the non-DESY members. We are very grateful to E. Elsen, R. Pöschl and H.-C. Schultz-Coulon for critical reading of the manuscript and many useful comments and suggestions which greatly improved this note. We are grateful to J. Coughlan, E. Elsen, T. Nicholls, H.-C. Schultz-Coulon and F. Sefkow for many helpful discussions during installation and operation of the L2TT. We like to mention H. Krehbiel for the outstanding development of the PQZP and Quickbus Receivers. We thank B. Heinemann, H. Itterbeck, D. Reyna, D. Schmidt and Y. Tsipolitis, for their contribution to the development of trig-

ger strategies and R. Stamen for his precious help during the operation of the L2TT. It is also a pleasure to thank all physicists, engineers and technicians, not listed as authors, who contributed to the project. We thank in particular B. Delcourt for early development of the Acquisition cards, J. Daubin for the ALTERA programming and the development of the Spy card, M. Bouchel for conception and test of the ASIC and V. Masbender for assembly and test of the PQZP and Quickbus Receiver cards.

## References

- [1] H1 Collaboration, I. Abt et al., Nucl. Instr. and Meth. A386 (1997) 310,  
H1 Collaboration, I. Abt et al., Nucl. Instr. and Meth. A386 (1997) 348
- [2] T. Nicholls et al., IEEE Trans. Nucl. Sci. **45**, No. 3 (1998) 810
- [3] J. Köhne et al., “Realization of a second level neural network trigger for the H1 Experiment at HERA”, Proceedings of AIHENP 96, Lausanne, World Scientific, 1996
- [4] J. C. Bizot et al., “Status of simulation for a topological level 2 trigger”, H1 Internal Note H1-02/92-212, unpublished (1992),  
J. C. Bizot et al., “Hardware study for a topological level 2 trigger”, H1 Internal Note H1-09/92-240, unpublished (1992)
- [5] “The HERA Luminosity Upgrade”, ed. U. Schneekloth, DESY HERA 98-05 (1998)
- [6] H1 SpaCal group, R. Appuhn et al., Nucl. Instr. and Meth. A386 (1997) 397,  
S. Spielmann, “L’électronique rapide de déclenchement du calorimètre SpaCal plomb/fibre-scintillante de l’expérience H1 à HERA”, Ph. D. Thesis, Ecole Polytechnique, Palaiseau, 1996
- [7] F. Sefkow et al., IEEE Trans. Nucl. Sci., Vol. 42, No. 4 (1995) 900
- [8] H. C. Schultz-Coulon et al., IEEE Trans. Nucl. Sci., Vol. 46, No. 4 (1999) 915
- [9] A. Campbell et al., IEEE Trans. Nucl. Sci., Vol. 39, No. 1 (1992) 255
- [10] W. Haynes, “Experiences at HERA with the H1 data acquisition system”, Proceedings of the Int. Conference on Computing in High Energy Physics 1992, Annecy, France, pp. 151-161
- [11] H1 Calorimeter Group, B. Andrieu et al., Nucl. Instr. and Meth. A336 (1993) 460
- [12] G. Molière, Zeitschrift für Naturforschung **2a**, 133–145 (1948); Zeitschrift für Naturforschung **3a**, 78–79 (1948)
- [13] Th. Wolff et al., Nucl. Instr. and Meth. A323 (1992) 537
- [14] S. Eichenberger et al., Nucl. Instr. and Meth. A323 (1992) 532
- [15] R. Eichler et al., “The first level MWPC trigger for the H1 detector”, H1 Internal Note H1-04/87-61, unpublished (1987)
- [16] J. Tutas, “A level 1 trigger from the limited streamer tube system”, H1 Internal Note H1-07/91-185, unpublished (1991)
- [17] T. Ahmed et al., Nucl. Instr. and Meth. A364 (1995) 456

- [18] F. Descamps, C. Vallée, “Data Acquisition for the H1 Calorimeters”, Proceedings of the III. Int. Conf. on Calorimetry in High Energy Physics, Corpus Cristi (1992),  
F. Blouzon, P. Nayman, J.-F. Huppert, L. Serot, “DSP/T0 Manuel Utilisateur”, Internal Note LPNHE Paris VI/VII, unpublished (1991)
- [19] C. Beigbeider and D. Breton, “The H1 PQZP System (Parallel Quickbus Zero-suppression Processor)”, H1 Internal Note H1-02/93-269, unpublished (1993)
- [20] High Performance ECL Data, Motorola, DL140/D, Rev. 4 (1996),  
H. Krehbiel, “Standards for the Transmission of Bit Data in the H1 Trigger System through Twisted-Pair Flat Cables”, H1 Internal Trigger Note No. 12/89, unpublished (1989)
- [21] H. Krehbiel, “The PQZP Receiver Card for the L2 Crates of H1”, H1 Internal Trigger Note No. 1/94, unpublished (1994)
- [22] ANSI/VITA 1-1994, American Nation Standard for VME64, VMEbus international trade association (VITA)
- [23] H. Krehbiel, “The L2 Crate of H1, tentative specifications”, H1 Internal Trigger Note No. 1/93, unpublished (June 1993)
- [24] Creative Electronic Systems, Switzerland, “VIC 8250 VMV to VME One Slot Interface User’s Manual” ver. 5.0, DOC 8250/UM, PN: 085.252,  
VICbus, VME Inter-Crate Bus, ISO/IEC JTC 1/SC26, ISO/IEC 11458  
▷ <http://www.ces.ch>
- [25] D. Hoffmann, Zwei-Elektron-Ereignisse im H1-Detektor, Ph. D. Thesis, University of Hamburg, DESY-THESIS-2000-001, 2000
- [26] C. Kleinwort, Manual for for H1NDB version 1.02/17, internal web document, unpublished
- [27] MOTOROLA MC68040 User’s Manual, Including the MC68040, MC68040V, MC68LC040, MC68EC040, and MC68EC040V, Motorola Inc. (1990), see also  
▷ <http://www.motorola.com>
- [28] Creative Electronic Systems, Switzerland, “FIC 8232, Fast Intelligent Controller, User’s Manual”, version 3.0 (1992)
- [29] ▷ <http://www.microware.com>
- [30] P. Mato, “OS-9 Buffer Manager - User’s Guide V2” CERN, unpublished (1988)
- [31] L. Guglielmi et al., “MEPHISTO - A Manageable and Efficient Package of HISTOgram for Data Acquisition under OS9/68k”, Laboratoire de Physique Corpusculaire, unpublished (1991)
- [32] E. Banaś and A. Ducorps, “L2TTMON - Monitoring Program for the L2 Topological Trigger in the H1 Experiment, User’s Guide”, INP Cracow Report Nr 1817/PH, unpublished (1999)

- [33] A. Ducorps, "TMacLib User's Guide", LAL, unpublished (1993)
- [34] R. Stamen, "Analyse Quasireeller QED-Compton-Ereignisse", Diplomarbeit Universität Dortmund, unpublished (1998),  
V. Lenderman, "Measurement of the QED Compton Scattering Cross Sections with the H1 Detector at HERA", Ph. D. Thesis, University of Dortmund, DESY-THESIS-2001-004, 2001
- [35] D. Schmidt, "Topologischer Trigger für inelastisch produzierte  $J/\psi \rightarrow e^+e^-$  am H1-Detektor bei HERA", Diplomarbeit Universität Hamburg, unpublished (1997)
- [36] B. Heinemann, "Measurement of Charged Current and Neutral Current Cross Sections in Positron-Proton Collisions at  $\sqrt{s} = 300$  GeV", Ph. D. Thesis University of Hamburg, DESY-THESIS-1999-046, 1999
- [37] H1 Collaboration, T. Ahmed et al., Phys. Lett. B 324 (1994) 241,  
S. Aid et al., Z. Phys. C 67 (1995) 565,  
S. Aid et al., Phys. Lett. B 379 (1996) 319,  
C. Adloff et al., Eur. Phys. Journal C 13 (2000) 609,  
C. Adloff et al., Eur. Phys. Journal C 19 (2001) 269
- [38] H1 Collaboration, C. Adloff et al., Phys. Lett. B 467 (1999) 156